ACS Catalysis
Research Article
pubs.acs.org/acscatalysis

Nanoporous Copper Films by Additive-Controlled Electrodeposition: CO_2 Reduction Catalysis

Thao T. H. Hoang,[†] Sichao Ma,[†] Jake I. Gold,[‡] Paul J. A. Kenis,[§,‡] and Andrew A. Gewirth*[,†,§]

[†]Department of Chemistry, University of Illinois at Urbana−Champaign, Urbana, Illinois 61801, United States

[‡]Department of Chemical & Biomolecular Engineering, University of Illinois at Urbana−Champaign, Urbana, Illinois 61801, United States

[§]International Institute for Carbon Neutral Energy Research (WPI-I2CNER), Kyushu University, Fukuoka 819-0395, Japan

Supporting Information

ABSTRACT: Electrodeposition from plating baths containing 3,5-diamino-1,2,4-triazole (DAT) as an inhibitor gives Cu films exhibiting high surface area and high CO_2 reduction activities. By changes in the pH and deposition current density, the morphologies of the Cu films are varied to exhibit wire, dot, and amorphous structures. Among these Cu films, the CuDAT-wire samples exhibit the best CO_2 reduction activities activity with a Faradaic efficiency (FE) for C_2H_4 product formation reaching 40% at −0.5 V vs RHE, a FE for C_2H_5OH formation reaching 20% at −0.5 V vs RHE, and a mass activity for CO_2 reduction at −0.7 V vs RHE of ∼700 A/g.

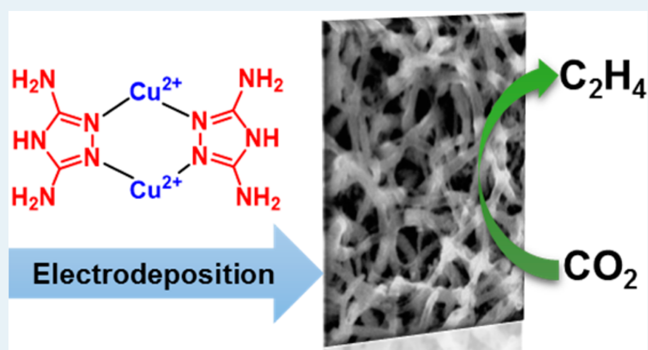

KEYWORDS: *CO_2 reduction, electrodeposition, copper, 3,5-diamino-1,2,4-triazole, ethylene*

1. INTRODUCTION

In a transition from fossil fuels to renewable energy, electrochemical energy conversion and energy storage play critical rolex. A key challenge to commercializing electrochemical energy conversion and storage systems is developing electrocatalysts with low cost, high activity, and high stability.[1] Many studies have focused on designing and controlling the morphology and compositions of either bulk catalysts (foil, disk, foam)[2−4] or nanoparticle catalysts.[1,4−7] While a bulk catalyst is easy to obtain, its activity is low due to the intrinsically small active surface area. Nanoparticles, while useful for schemes that seek to minimize precious-metal usage and increase active surface area, are harder to fabricate and require a binder when they are utilized in a real electrolyzer, the presence of which can inhibit reactivity, particularly when accompanied by substantial gas and/or product evolution.[8,9]

Recently, we fabricated Ni and NiFe catalysts for the oxygen evolution reaction (OER) by electrodepositing these materials in the presence of 3,5-diamino-1,2,4-triazole (DAT) as a deposition additive. The resulting nanostructured electrodeposit is a very active catalyst for the OER.[10] However, these "additive-controlled" electrodeposited Ni and NiFe films do not exhibit a well-defined morphology because the electrodeposition process occurs simultaneously with vigorous H_2 evolution. We wondered whether our electrodeposition method could be used to control the morphology of a nanostructured film produced under gentler conditions. We also wondered whether our electrodeposition method could be suitable for other transition metals exhibiting electrocatalytic activity.

A promising transition metal for both electrodeposition and electrocatalysis is Cu. Cu has a long history of electrodeposition in microelectronics contexts.[11,12] Cu is also used as an electrocatalyst for CO_2 and NO_3^- reduction.[13−22] Substantial effort has been extended to fabricate Cu nanoparticles and Cu foams, some of which exhibit high catalytic activity for CO_2 reduction.[2,6,23] While nanoparticles exhibit high active surface area and hence high activity, their activity and stability are limited by the requirement for a binder to adhere the particles to an electrode. Metal foams with high porosity could be a way to provide a high-surface-area catalyst without the requirement of any binder.[2,8] However, most metal foams are made either by a metallization process on a foam substrate[24] or by electrodeposition using hydrogen bubbles as the template.[2,23,25,26] Metal foams made by metallization on a foam substrate are expensive and are limited to the structures of available foam substrates. While the hydrogen bubble templating method has the advantages of simplicity and low cost, the presence of vigorous hydrogen bubble evolution and the fast rate of deposition under high potential or current during foam synthesis puts constraints on the tunability of the film structure and potentially compromises film stability, particularly at high

Received: December 20, 2016
Revised: March 17, 2017
Published: March 22, 2017

Downloaded via UNIV ILLINOIS URBANA-CHAMPAIGN on August 21, 2022 at 22:56:15 (UTC).
See https://pubs.acs.org/sharingguidelines for options on how to legitimately share published articles.

ACS Publications © 2017 American Chemical Society

DOI: 10.1021/acscatal.6b03613
ACS Catal. 2017, 7, 3313−3321

loading.[2,16,23] A new method of fabricating metal foams for electrocatalysis applications is desired.

Electrochemical reduction of CO_2 into value-added chemicals has attracted increasing attention for decades due to its potential to facilitate a sustainable redox cycle for intermittent renewable energy conversion and storage.[13,19,20] Among the many catalysts for CO_2 reduction, Cu is the only known metal catalyst able to generate various products—particularly hydrocarbons and oxygenates—and tune their relative quantities and Faradaic efficiencies (FEs) by changing the structure and morphology of Cu catalysts.[3,6,19,20,27−32] Recently, Cu nanofoams have been reported that showed interesting results for CO_2 reduction.[2] These Cu nanofoams exhibited enhancement in Faradaic efficiency of HCOOH (up to 37%) in comparison to those obtained from smooth Cu. However, the main product is H_2 (50−90% FE), leading to a low total CO_2 reduction efficiency to desirable products of 10−50%. While these Cu nanofoams were shown to be highly porous, the total observed reduction current density was only 2−2.6 times higher than those obtained from smooth Cu.[2]

In this paper we exploit our electrodeposition method to synthesize Cu films with high surface area and tunable morphology. We evaluate the ability of these films as catalysts for CO_2 electrodreduction. Remarkably, we find these films to be among the most active for CO_2 reduction on a Cu catalyst.

2. EXPERIMENTAL SECTION

2.1. Electrodeposition of Metal. The Cu plating baths were made from 0.1 M $CuSO_4{\cdot}5H_2O$ and 10 mM of additive, with the pH adjusted between pH 1 and 3 by using H_2SO_4. The concentration of additive was optimized at 10 mM in order to obtain a uniform deposit and well-defined morphology. The additives tested were 3,5-diamino-1,2,4-triazole (DAT), dodecyltrimethylammonium bromide (DTAB), and thonzonium bromide (ThonB, hexadecyl[2-[(4-methoxyphenyl)-methylpyrimidin-2-ylamino]ethyl]dimethylazanium bromide), all of which were obtained from Sigma-Aldrich. Cu was electrodeposited galvanostatically at a constant current density ranging from 1 to 4 mA/cm^2 until a final deposition charge was reached (typically 2 C/cm^2, unless otherwise stated). Pt wire was used as the counter electrode. The counter electrode was separated from the working electrode by using an ion exchange membrane (Fumatech FAP-375-PP) in a two-compartment electrochemical cell to avoid oxidation of additives at the counter electrode. A "leakless" Ag/AgCl (eDAQ) electrode was placed near the working electrode to measure the potential.

Substrates for electrodeposition were cleaned just before use. Au (200 nm thickness, fabricated on one side of glass cover slips by e-beam deposition) was rinsed with Milli-Q water and then flamed under H_2. Cu foil (Sigma-Aldrich, thickness 0.125 mm, purity 99.9) was rinsed thoroughly with Milli-Q water. Carbon paper (GDL, Sigracet 35 BC, Ion Power) was activated either by immersing in concentrated HNO_3 for 1 h or using an electron beam coated with ∼10 nm of Cu (∼0.01 mg/cm^2). Carbon paper pretreated by both methods exhibits similar morphologies and electrochemical activities.

For flow cell electrolysis experiments, Cu was electrodeposited on carbon paper and used as a gas diffusion electrode. However, HNO_3 treatment causes both sides of the carbon paper to become hydrophilic and allows liquid to easily pass through, which causes flooding of electrolyte into the gas chamber. Thus, the carbon paper was sputter-coated with Cu instead of being treated with HNO_3 before electrodeposition. Then 2 C/cm^2 of Cu was electrodeposited on the 1 × 2.5 cm section of carbon paper.

2.2. Materials Characterization. The amount of Cu electrodeposited was measured by ICP-OES (PerkinElmer 2000 DV optical emission spectrometer). Scanning electron microscope (SEM) images were obtained from a Hitachi A-4700 high-resolution microscope. X-ray photoelectron spectroscopy (XPS) was performed with a Physical Electronics PHI 5400 instrument. The thickness of the electrodeposited film was measured by surface profilometry (Sloan Dektak).[3]

2.3. Electrochemical Measurements for CO_2 Reduction. Cyclic voltammetry (CV), chronoamperometry (CA), and chronopotentiometry (CP) evaluating CO_2 reduction were performed at room temperature using a CHI 760D or Biologic SP-150 potentiostat with a Pt-mesh counter electrode and an Ag/AgCl reference electrode. Before the electrochemical measurement, the electrolyte (1 M $KHCO_3$) was saturated with CO_2. The Ag/AgCl reference electrode was calibrated before each experiment with a normal hydrogen electrode (NHE) in 1 M $HClO_4$. Potentials are reported with respect to the reversible hydrogen electrode (RHE), unless otherwise stated. All voltammetry data were *iR* corrected. Flow cell measurements and product characterization were performed as previously reported.[6] The pH of the electrolyte at the inlet of the flow cell was 13.5, and the pH at the outlet was 13.3.

3. RESULTS AND DISCUSSION

3.1. Effects of Additives on Cu Deposition. Figure 1a shows CVs obtained from Au substrates in solutions containing

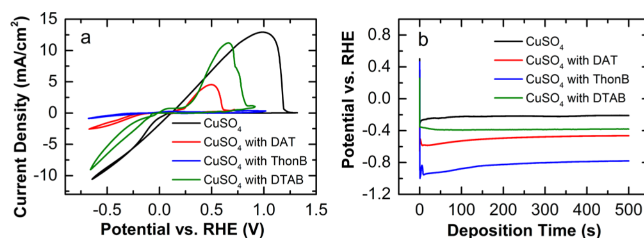

Figure 1. Influence of additives (a) on the CV of Cu redox reaction (scan rate 10 mV/s) and (b) on the chronopotentiometry at −4 mA/cm^2 of a Au substrate in a copper electrodeposition bath of 0.1 M $CuSO_4$ at pH 2 with and without 0.01 M additives (DAT, ThonB, DTAB).

0.1 M $CuSO_4$ at pH 2 with and without 0.01 M of different additives. In the absence of an additive, the voltammetry shows a strong cathodic feature commencing at ∼0.11 V vs RHE associated with the onset of bulk Cu deposition. Upon addition of 0.01 M DAT, Cu deposition is inhibited until a potential of −0.18 V vs RHE is reached (η = 0.25 V). The reverse scan exhibits negligible hysteresis, showing that the inhibitor does not break down at negative potentials. At positive potentials, voltammetry obtained in the absence of DAT shows a substantial anodic feature associated with oxidation of the deposited Cu. Addition of DAT leads to a slightly higher overpotential for Cu oxidation, indicating that DAT is adsorbed on the surface at these potentials.

Figure 1b shows the electrodeposition profile of Cu on Au substrates in solutions containing 0.1 M $CuSO_4$ at pH 2 with and without DAT for 500 s. A deposition current of −4 mA/cm^2 was maintained at ∼−0.2 V without DAT and at −0.5 V vs RHE with DAT. CP and CV both indicate that DAT inhibits

DOI: 10.1021/acscatal.6b03613
ACS Catal. 2017, 7, 3313−3321

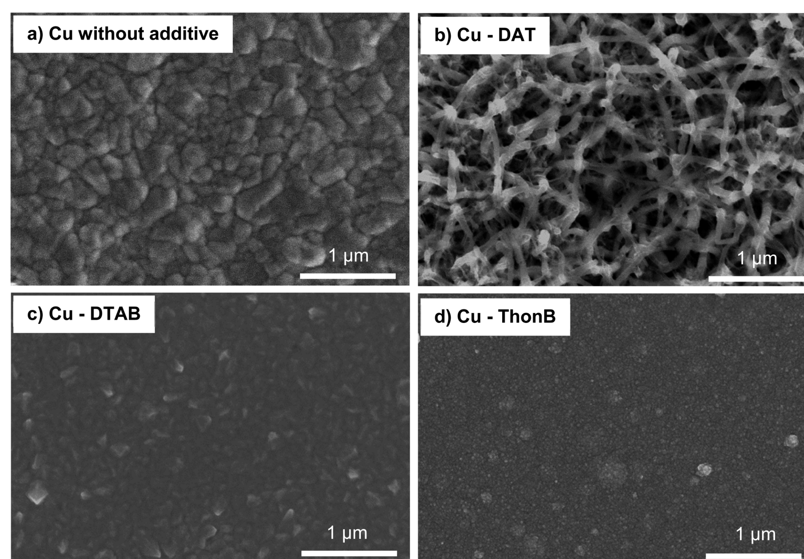

Figure 2. SEM images of Cu electrodeposited (a) without additive, (b) with DAT, (c) with DTAB, and (d) with ThonB.

Cu deposition. ICP-OES data show that the Coulombic efficiency of Cu electrodeposited in the additive-free solution is ~80%, while the Coulombic efficiency of Cu electrodeposited with DAT is ~50%. The low deposition efficiency of solutions containing DAT once again indicates that DAT inhibits Cu electrodeposition. Both the O_2 reduction reaction and/or the H_2 evolution reaction probably occur during the Cu electrodeposition process. However, the effects of the H_2 evolution reaction on the morphology of Cu deposition is not as obvious as that found in Cu films electrodeposited using the H_2 bubble template method.[2,33] We did not see any bubbles associated with H_2 evolution during deposition, we see no large pores (micrometer sized or larger) arising from H_2 bubble templating,[2,33] and the cracked surfaces usually seen with attendant H_2 evolution were also not in evidence. More to the point, the Coulombic efficiency (CE) of the Cu deposition was ~50%, much higher than the ~15% we found during Ni deposition in a previous paper[10] where H_2 evolution definitely occurred and controlled the deposit morphology. Our 50% CE is also larger than the ~20% reported during the synthesis of Cu foams where Cu is electrodeposited with a H_2 bubble template.[2,33]

Upon the addition of ThonB and DTAB, Cu deposition is inhibited at overpotentials of 0.35 and 0.15 V, respectively.[34] ThonB exhibits the strongest inhibitive effect on Cu deposition among the three additives, showing both a large overpotential and low deposition/stripping current density. In contrast, DTAB exhibits a higher current density and a lower overpotential for deposition onset.

Figure 2 shows SEM micrographs of Cu films electrodeposited with and without additives. Interestingly, while the Cu films electrodeposited with DAT (Figure 2b) exhibit a rough and porous surface, Cu films electrodeposited without additive (Figure 2a), with DTAB (Figure 2c), and with ThonB (Figure 2d) all exhibit smooth surfaces. In the presence of DTAB and ThonB, Cu films exhibit an even smoother surface than that in the absence of additives. All three additives inhibit Cu deposition, but ThonB and DTAB apparently act as deposition levelers as expected,[34] while DAT addition results in a rough surface. Interestingly, while UV−vis spectra obtained from solutions containing DAT and Cu exhibit the presence of what is likely a ligand-to-metal charge transfer (LMCT) band confirming DAT-Cu coordination, such a feature is not present for solutions containing either DTAB or ThonB and Cu (Figure S1 in the Supporting Information). The more facile coordination between Cu and DAT likely results from the presence of N coordination sites in DAT that are absent in the other two additives. Thus, while all three additives inhibit Cu deposition, only DAT coordinates to Cu, inhibiting surface diffusivity.

3.2. Effects of pH and Deposition Current on Electrodeposition of Cu with DAT. In order to evaluate the effect of DAT protonation on Cu electrodeposition, we examined Cu deposition with DAT at different pH values. Figure 3 shows the electrodeposition profile of Cu on Au

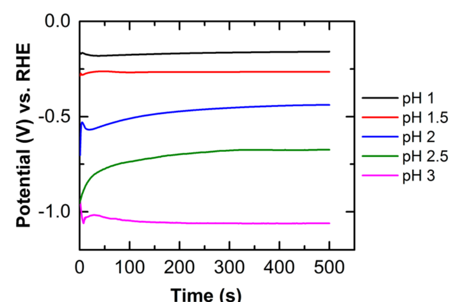

Figure 3. Influence of pH on the deposition of Cu on an Au substrate in an electrodeposition bath containing 0.1 M $CuSO_4$ + 0.01 M DAT at i = −4 mA/cm^2.

substrates in solutions containing 0.1 M $CuSO_4$ and 0.01 M DAT at pH 1, 1.5, 2, 2.5, and 3, values less than the pK_a for DAT of 4.43.[35] Increasing the pH from 1 to 3 resulted in an increase of ~0.9 V in deposition potential. This phenomenon suggests that inhibition of DAT increases with increasing pH. A solution of 0.1 M $CuSO_4$ and 0.01 M DAT at pH 1 exhibits a blue color similar to that found in a solution containing $CuSO_4$ without DAT. As the pH is raised from pH 1 to pH 3, the solution changes from blue to green. Additionally, the solution starts to become cloudy at pH 3, indicating the presence of precipitates in the solution. Thus, the increased inhibition of

DOI: 10.1021/acscatal.6b03613
ACS Catal. 2017, 7, 3313−3321

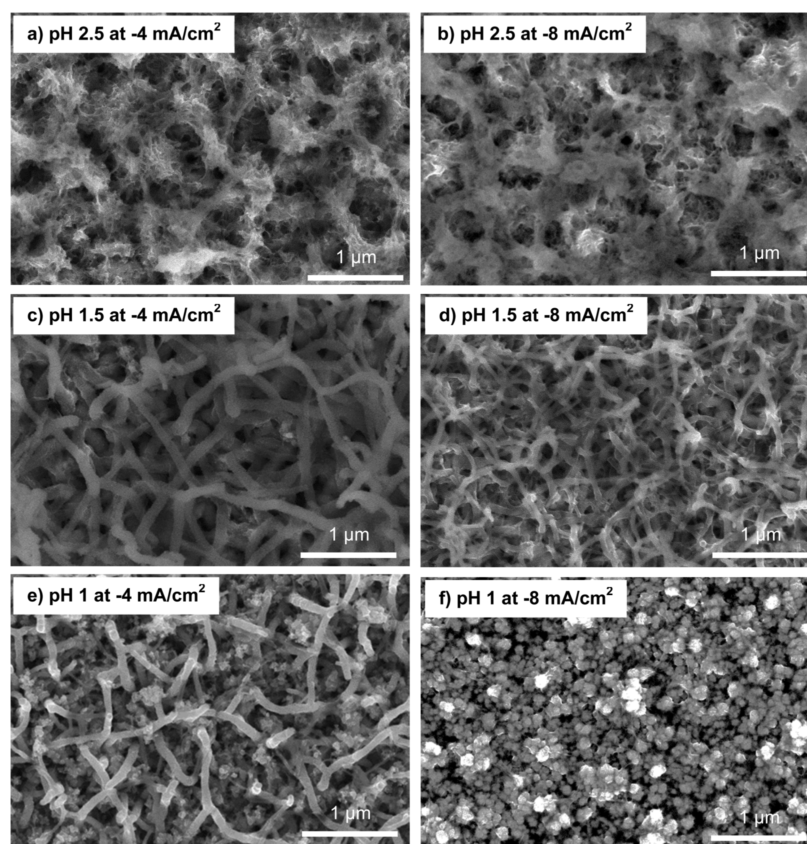

Figure 4. SEM micrographs of Cu films deposited in 0.1 M CuSO4 and 0.01 M DAT solution at (a) pH 2.5 at −4 mA/cm^2, (b) pH 2.5 at −8 mA/cm^2, (c) pH 1.5−2 at −4 mA/cm^2, (d) pH 1.5−2 at −8 mA/cm^2, (e) pH 1 at −4 mA/cm^2, and (f) pH 1 at −8 mA/cm^2.

Table 1. Parameters of Cu Samples Obtained from 0.1 M $CuSO_4$ Deposition Baths

sample	amt of DAT, mM	pH	I_{depo}, mA/cm^2	morphology	loading,[a] mg/cm^2	thickness,[b] μm	density,[c] g/cm^2	crystallite size,[d] nm	A_{active}/$A_{geometric}$[e]
Cu foil				smooth			8.96		1
Cu-poly		2.0	−4	smooth	0.53 ± 0.03	0.60 ± 0.05	~8.8	19.5 ± 3.0	~1
CuDAT-amorphous	10	2.5	−4	amorphous	0.29 + 0.04	180 ± 0.25	~1.6	2.2 ± 15	~6
CuDAT-dot	10	1.0	−8	dot	0.31 ± 0.03	0.70 ± 0.10	~4.4	9.5 ± 13	~5
CuDAT-wire	10	1.5	−4	wire	0.28 ± 0.03	1.75 ± 0.20	~1.6	4.6 ± 9	~7

[a]Loading measured by ICP-OES. [b]Thickness of electrodeposited film measured by surface profilometry. [c]Density calculated from loading per cm^2 and thickness of the film. [d]Crystallite size calculated from XRD patterns using the Scherer equation. [e]Active surface area calculated from Pb_{UPD} experiments.

DAT with increasing pH likely results from the more facile formation of Cu-DAT complexes, a result corroborated by UV−vis spectroscopy (Figure S2 in the Supporting Information). Deposition solutions at pH higher than 3 did not yield reproducible and uniform deposits.

Figure 4 shows SEM micrographs of Cu electrodeposits obtained with DAT at (a) pH 2.5 at −4 mA/cm^2, (b) pH 2.5 at −8 mA/cm^2, (c) pH 1.5 at −4 mA/cm^2, (d) pH 1.5 at −8 mA/cm^2, (e) pH 1 at −4 mA/cm^2, and (f) pH 1 at −8 mA/cm^2. Clearly different types of deposits are formed as a function of different pHs and current densities. At pH 2.5, the Cu deposit exhibits particles of ill-defined shape at deposition currents of −4 and −8 mA/cm^2 (Figure 4a,b). At pH 1.5 (Figure 4c,d), the deposit exhibits a wirelike shape, with wire diameters of 50−70 nm. At pH 1 the Cu films exhibit a dot shape (Figure 4f) or a mixture of wire and dot shapes (Figure 4e). Thus, the pH has a strong effect on the nanostructure shape and density of the whole film, a result likely explained by the differences in Cu coordination at these different pH values. At low pH where the deposited Cu particles exhibit a well-defined shape (pH 1.5 and 1), deposition currents show clear effects on particle size. On comparison of the Cu film deposited at 4 mA/cm^2 and pH 1 (Figure 4c) and the film deposited at 8 mA/cm^2 and pH 1 (Figure 4d), the Cu film deposited at 4 mA/cm^2 shows larger and longer wirelike particles than the film deposited at 8 mA/cm^2. This result suggests that higher deposition currents increase the nucleation density of Cu, resulting in smaller-sized Cu nanostructures.[36]

The mechanism by which DAT modifies the electrodeposition process to yield the rough and porous Cu surfaces observed can be explained by invoking a diffusion-limited aggregation (DLA) process,[37−39] similar to what we reported for NiDAT and NiFeDAT deposits recently.[10] In the Cu case, DAT binds to the substrate surface, reducing the number of

DOI: 10.1021/acscatal.6b03613
ACS Catal. 2017, 7, 3313−3321

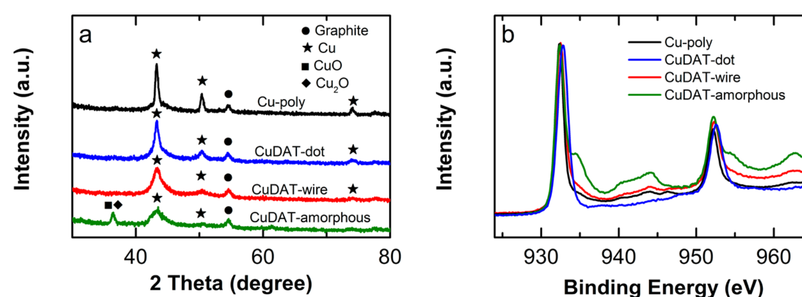

Figure 5. (a) XRD and (b) XPS patterns of Cu-poly, CuDAT-dot, CuDAT-wire, and CuDAT-amorphous.

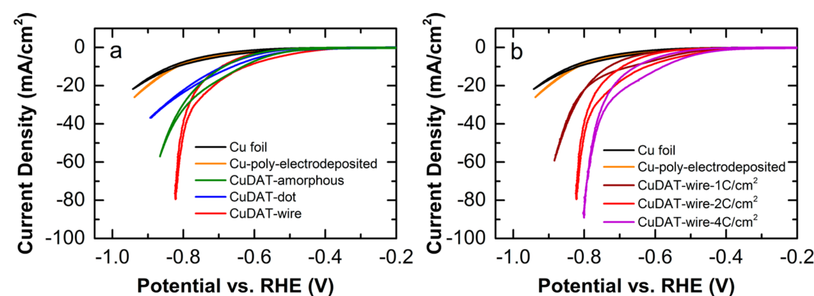

Figure 6. CV in an H-cell at a scan rate of 50 mV/s (*iR* corrected) in 1 M $KHCO_3$ saturated with CO_2 (a) from Cu foil, Cu-poly electrodeposited without DAT, CuDAT-dot, CuDAT-amorphous and CuDAT-wire and (b) from Cu foil, Cu film electrodeposited without DAT, and CuDAT-wire samples with deposition charges of 1, 2, and 4 C/cm^2.

nucleation sites for Cu deposition, thus initiating roughness. These rough areas experience a high local current density and grow exponentially, while other areas are still DAT-covered and diffusion-inhibited. The growth of the deposit is further inhibited by the coordination of DAT to Cu, limiting subsequent diffusion both before and after reduction. As shown above, the inhibition of DAT is controlled by changing the pH of the deposition solution along with the deposition current density.

In the previously reported NiDAT and NiFeDAT cases,[10] the high surface roughness arises as a consequence of both inhibition of electrodeposition by DAT and H_2 adsorption on the electrode surface. In the Cu case studied here, however, the high surface roughness involves only DAT coordination, without formation and adsorption of H_2. The absence of vigorous H_2 bubbling during CuDAT electrodeposition could explain why cracks—clearly in evidence with the NiDAT and NiFeDAT films[10]—are not found in the Cu films reported here.

Through SEM images of the electrodeposited films obtained at different pHs and different deposition current densities, we found that by controlling these parameters we could control the morphology of the Cu films. When the pH decreases from 2.5 to 1, DAT association to the substrate surface is weaker, resulting in a dense film with larger particle sizes relative to films deposited at higher pH (Table 1). At pH 2.5 (Figure 4e,f), DAT binds strongly on the substrate surface, resulting in smaller particle size (Table 1). However, Cu and Cu oxides formed at the same time at this pH caused an ill-defined shape of the film. At higher current density, the growth is faster and so thinner wire structures are obtained. Through control experiments we showed that the morphology of the CuDAT films is not dependent on the substrate (Figures S3−S10 in the Supporting Information).

3.3. Characterization of Cu Films. Figure 5a shows the XRD patterns of Cu-poly electrodeposited without DAT, as well as CuDAT-dot, CuDAT-wire, and CuDAT-amorphous, all electrodeposited with DAT. While Cu-poly, CuDAT-dot, and CuDAT-wire samples show only Cu peaks at $2\theta = 43.46°$ (from Cu (111)), 50.62° (from Cu (200)), and 74.40° (from Cu (220)), CuDAT-amorphous samples electrodeposited at higher pH than other samples show an extra peak at $2\theta \approx 36°$, which is associated with Cu oxides (Cu_2O and/or CuO). The presence of Cu oxides in CuDAT-amorphous is also evident from a series of satellite peaks[40−42] in the XPS pattern shown in Figure 5b.

The Cu peaks in XRD patterns of CuDAT samples are broader and have lower intensity than the Cu-poly sample, indicating that CuDAT samples exhibit a smaller crystallite size than Cu-poly. The specific crystallite size of each sample, determined by the Scherer equation, is summarized in Table 1. The density (loading/(area × thickness)) of Cu-poly samples is similar to that of Cu foil. In contrast, the density of CuDAT-dot samples is ∼50% of the Cu foil density, while the density of CuDAT-wire and CuDAT-amorphous is ∼18% of that of Cu foil. The electroactive surface area of the different Cu samples was measured by using Pb underpotential deposition (Pb_{UPD}) to form a conformal coat on the accessible Cu deposit[43,44] (Figure S11 and Table S1 in the Supporting Information). The results (Table 1) show that the Cu-poly sample electrodeposited without DAT exhibits a Pb_{UPD} charge similar to that from Cu bulk samples: i.e., the electroactive surface area is close to the geometric area.[44] This result is not unexpected, as we found previously that polished Cu-poly electrodes exhibit roughness values very similar to those from single crystals.[45] Alternatively, the CuDAT samples exhibit a higher active surface area than Cu-poly, while the CuDAT-wire samples exhibit the highest active surface area among the tested samples, around 7 times higher than that of the Cu-poly samples.

The low densities and high surface areas found for the CuDAT samples suggest that they could be considered thin

DOI: 10.1021/acscatal.6b03613
ACS Catal. 2017, 7, 3313−3321

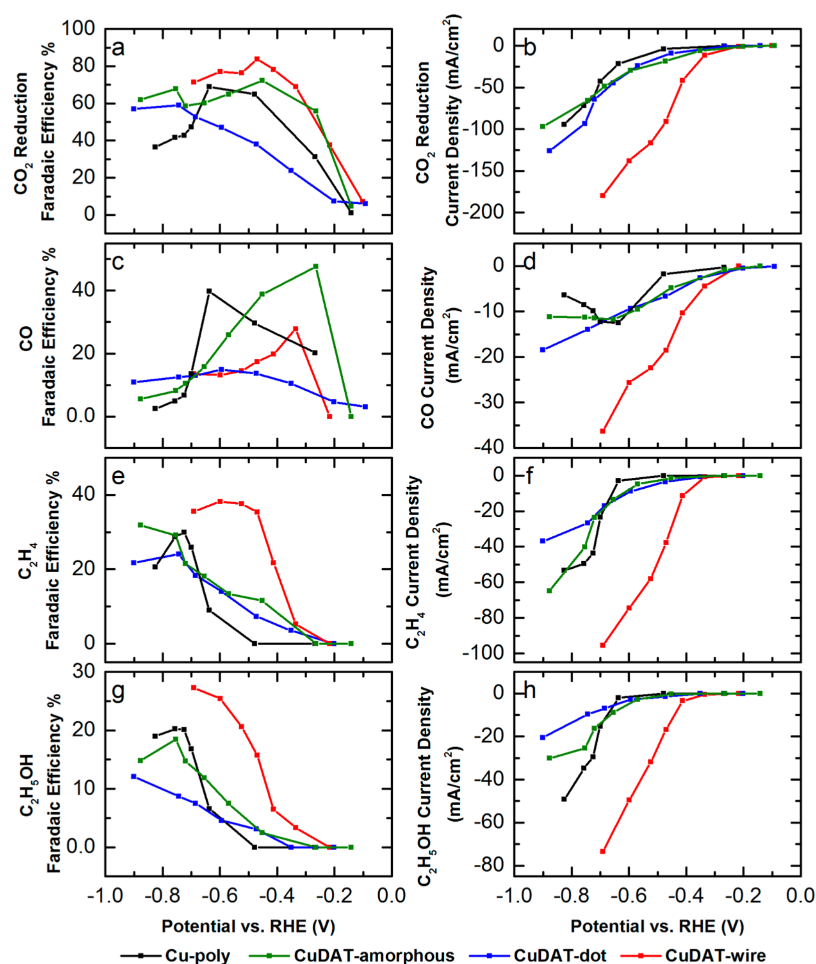

Figure 7. Faradaic efficiencies and corresponding current densities for (a, b) total CO_2 reduction, (c, d) CO production, (e, f) C_2H_4 production, and (g, h) C_2H_6OH production with 1 M KOH electrolyte in an electrolysis flow cell.

metallic foams. However, the pore density and pore size are difficult to determine for these materials. The active surface area of these materials is significantly higher than their geometric area, suggesting that these materials are open-cell foams, which allow gas and electrolyte to transfer through the material to interact with deeper layers.

3.4. Electrochemical Reduction Activity of Cu Films in an H-Cell. Open-cell metallic foam is known to increase the catalytic activity of electrochemical systems due to its high surface area and permeability.[46,47] We evaluated the catalytic activity of our CuDAT samples for the CO_2 reduction reaction. Figure 6a shows an *iR* corrected CV obtained from Cu and CuDAT samples in 1 M $KHCO_3$ saturated with CO_2 using an electrochemical H-cell. Reduction currents are associated with CO_2 reduction and H_2 evolution. The Cu foil and Cu-poly films electrodeposited without DAT (control samples) exhibit low activity in this potential region. In contrast, CuDAT samples exhibit lower onset and much higher reduction currents than the Cu-poly or Cu foil. CuDAT samples exhibit a reduction onset at around −0.6 V vs RHE, while the onsets of the Cu-poly and Cu foil are around −0.8 V vs RHE. The CuDAT-wire sample exhibits the highest reduction current density. Stability tests show that CuDAT samples maintain their catalytic activity for at least 8 h (Figure S12 in the Supporting Information).

The increased activity of the CuDAT samples in comparison to the Cu-poly sample might be explained by the increase in surface area of the catalysts. In particular, the current density exhibited by the CuDAT-wire sample is 6 times (at low potential) to 9 times (at high potential) larger than the current density from Cu-poly. The overall increase is consistent with the Pb_{UPD} measurements, where the active surface of the CuDAT-wire sample is shown to be 7 times larger than that of the Cu-poly sample. The small mismatch here suggests that (a) the current densities of the catalysts are dependent not only on surface area but also on diffusion of CO_2 in and products out of the catalyst (which is different with different catalysts and different at different potentials) and/or (b) Pb_{UPD} is not a perfect method with which to measure surface area for porous materials (in particular, Pb diffusion is slow and the lower Pb concentration in confined areas might result in a shifting potential for UPD).[48]

Next, we evaluated the effects of Cu loading on the CO_2 reduction rate. Figure 6b shows that Cu-poly electrodeposited without DAT and Cu foil both exhibit similar CO_2 reduction activities, indicating that CO_2 reduction is a surface process and is independent of Cu film thickness. However, the CO_2 reduction activity of CuDAT-wire samples is related to the deposition charge: i.e., Cu loading. Figure 6b shows that as the loading is increased (from 1 to 4 C/cm^2), the CO_2 reduction current density also increases. This behavior suggests that the surface area of the CuDAT-wire film increases while it maintains porosity and permeability with high loading. CuDAT-wire reaches −90 mA/cm^2 at ∼−0.8 V vs RHE,

DOI: 10.1021/acscatal.6b03613
ACS Catal. 2017, 7, 3313−3321

which is 6−10 times higher than the current density observed for Cu foam catalysts reported previously.[2,3,23,49]

3.5. CO_2 Reduction Reaction Activity and Product Distribution of Cu Films in a Flow Cell. To evaluate the gas permeability of the CuDAT film and the relationship between its catalytic activity and product distribution during CO_2 reduction, we also tested CuDAT samples in a flow cell.[6] The 1 M KOH alkaline media was used to increase the electrolyte conductivity (in comparison to other electrolytes such as $KHCO_3$ and K_2SO_4) and improve the CO_2 reduction reaction kinetics by suppressing H_2 evolution, as described in prior work.[6,50,51] Figure 7 shows the Faradaic efficiency (FE) and partial current density for total CO_2 reduction and all major products (CO, C_2H_4, and C_2H_5OH) using Cu-poly electrodeposited without DAT, CuDAT-amorphous, CuDAT-dot, and CuDAT-wire in a 1 M KOH electrolyte as a function of cathode potential. Specific values for cathode potential and Faradaic efficiencies for all products are given in Table S2 in the Supporting Information). In this study the CuDAT-wire sample exhibits a relatively high total CO_2 reduction current density as well as partial current density and FE for CO, C_2H_4, and C_2H_5OH at low cathode overpotentials.

Furthermore, CuDAT-wire exhibits a higher total CO_2 reduction FE and current density relative to CuDAT-amorphous, CuDAT-dot, and Cu-poly (Figure 7a,b). During CO_2 reduction measurements of the CuDAT-wire (with high porosity and low density; see Figure S3 in the Supporting Information), few or no gas bubbles emerged from the electrolyte chamber, suggesting that the CuDAT-wire samples have good gas permeability for CO_2 into and products out of the electrolyte chamber. Cu-poly samples, in which particles do not cover the whole electrode surface (see Figure S9 in the Supporting Information), also show good gas permeability. However, a large portion of the current is associated with H_2 evolution and non-Faradaic processes from that part of the carbon substrate not covered by the Cu-poly catalyst, leading to low total FE (Table S2 in the Supporting Information) in this case. Both CuDAT-amorphous and CuDAT-dot catalysts cover the whole electrode surface as a low-porosity film (Figure S8 in the Supporting Information). Consequently, these materials have poor gas permeability, which explains both the low CO_2 reduction current and low FE of these catalysts relative to the CuDAT-wire films.

Figure 7c,d shows that, for all catalysts, CO formation starts at ∼−0.2 V and increases at more negative cathodic overpotentials. The FE for CO of CuDAT-wire and CuDAT-amorphous reaches a maximum value of ∼40% at ∼−0.3 V vs RHE, which is much better than that found for the Cu-poly and CuDAT-dot samples. At potentials <−0.3 V the FE for CO production decreases while the FEs associated with C_2 products, including C_2H_4 (Figure 7e, 7f) and C_2H_5OH (Figure 7g,h), starts to increase. A possible explanation for this trend is that adsorbed CO is an important intermediate for the formation of C_2 products, as has been suggested previously.[6,18−20,52,53] The FE for C_2H_4 production (Figure 7e) for the CuDAT-wire catalyst reaches and maintains a maximum value of ∼40% at a potential of −0.5 V vs RHE, which is a higher FE at a smaller overpotential relative to what is observed for the other Cu samples considered here. The CuDAT-wire catalyst also exhibits the highest FE and current density for C_2H_5OH production (Figure 7g) at overpotential lower than that for the other catalysts. The high activity for C_2 products of CuDAT-wire is comparable to that of Cu−Cu oxide nanoparticle catalysts which we reported recently.[6] The current density of CuDAT-wire is 6−10 times higher than that of of other reported Cu catalysts in an H-cell[2,3,23,49] and more than 20 times higher than that of other Cu nanoparticle catalysts in a similar flow cell.[30] Interestingly, the CuDAT samples utilized here feature about 3 times lower Cu loading (∼0.3 mg/cm^2) relative to the loadings utilized in other Cu systems (typically ∼1 mg/cm^2), suggesting that the catalytic activity with respect to catalyst loading, i.e. the mass activity, of the CuDAT systems studied here is very high (Figure S13 in the Supporting Information). In particular, the mass activity for CO_2 reduction of CuDAT-wire at −0.7 V vs RHE is ∼700 A per gram of Cu, which to the best of our knowledge is among the best mass activities found from a Cu catalyst performing CO_2 reduction.

The catalytic activity normalized with respect to the electrochemically active surface area (measured by Pb_{UPD}) in the H-cell (Figure S14a in the Supporting Information) shows that all Cu-poly and CuDAT catalysts exhibit similar reduction current densities. Only in the flow cell (Figure S14b) does the CuDAT-wire catalyst exhibit ∼2 times higher CO_2 reduction current density relative to the other Cu-poly and CuDAT catalysts, which is likely due to the better gas permeability through the CuDAT-wire relative to the others.

The XRD data, reported in Figure 5, show that the (111)/(200) ratios of Cu-poly, CuDAT-dot, CuDAT-wire, and CuDAT-amorphous are ∼5.1, ∼5.2, ∼5.9, and ∼25, respectively. Single-crystal Cu catalysts such as Cu (200)[54] and Cu (200) combined with Cu(111) or Cu(110)[55] have been also reported to promote ethylene formation. Because the (111)/(200) ratios for Cu-poly, CuDAT-dot, CuDAT-wire are similar, the relative effects of different planes on the product distribution of CO_2 reduction should be similar as well. However, the current densities and product distributions for CO_2 reduction of Cu-poly, CuDAT-dot, and CuDAT-wire are quite different (Figure 7). Additionally, although CuDAT-amorphous and CuDAT-dot exhibit significant differences in their (111)/(200) ratios, their current densities and product distributions are quite similar (Figure 7). This result suggests that the differences in distribution of planes in our catalysts are not the main origin of differences in their catalytic activity. Rather, the XRD data show that the width of the planes is much smaller in the CuDAT samples relative to Cu-poly. In turn, this suggests the presence of increased step density on these materials relative to Cu-poly. The enhancement in C_2 product formation (both FE and current density) probably can be explained by the effect of "nanosize" CuDAT particles. The nanoporous CuDAT surfaces give rise to steps and edges with low-coordinated Cu atoms, which have been postulated to be more active toward the reduction of CO_2 to C_2 products: steps and edges along with terraces promote adsorption of C_1 intermediates and facilitate their dimerization to form C_2 products.[3,19,52,55−57] Indeed, Hori showed that both (220) and (111) features were required to obtain the highest activity for hydrocarbon production on Cu.[55]

4. CONCLUSION

We developed a facile method to electrodeposit high-surface-area Cu films onto conductive substrates. Our method relies on the inhibition of nucleation through the presence of an additive, DAT, the degree of which is controlled by pH and current density. The films exhibit active areas many times larger than that found absent the deposition additive. In contrast to porous Cu films made by exploiting H_2 bubbling during electro-

DOI: 10.1021/acscatal.6b03613
ACS Catal. 2017, 7, 3313−3321

deposition, our films exhibit small and stable pores and the resulting structures are tunable, depending on deposition conditions. We showed that the electrodeposited Cu films exhibit high activity for CO_2 reduction, resulting in the facile production of C_2H_4 and C_2H_5OH. Moreover, the films are stable and maintain their activity over a a time scale of several hour times. The mass activity for CO_2 reduction of CuDAT-wire is as high as ~700 A/g at −0.7 V vs RHE. While we focused on CO_2 reduction activity here, the ability to tune the nature of the Cu electrodeposit raises interesting possibilities for controlling and enhancing the (electro)catalytic activity of other metals.

■ ASSOCIATED CONTENT

Supporting Information

The Supporting Information is available free of charge on the ACS Publications website at DOI: 10.1021/acscatal.6b03613.

Relevant figures and procedure as noted in the text (PDF)

■ AUTHOR INFORMATION

Corresponding Author

*A.A.G.: e-mail, agewirth@illinois.edu; tel, 217-333-8329; fax, 217-244-3186.

ORCID

Paul J. A. Kenis: 0000-0001-7348-0381

Andrew A. Gewirth: 0000-0003-4400-9907

Notes

The authors declare no competing financial interest.

■ ACKNOWLEDGMENTS

This work was supported by the NSF (Grant CHE-1309731), which is gratefully acknowledged. We also acknowledge the International Institute for Carbon Neutral Energy Research (WPI-I2CNER), which is sponsored by the World Premier International Research Center Initiative (WPI) of the MEXT in Japan.

■ REFERENCES

(1) Guo, Y. G.; Hu, J. S.; Wan, L. J. *Adv. Mater.* **2008**, *20*, 4384.
(2) Sen, S.; Liu, D.; Palmore, G. T. R. *ACS Catal.* **2014**, *4*, 3091.
(3) Tang, W.; Peterson, A. A.; Varela, A. S.; Jovanov, Z. P.; Bech, L.; Durand, W. J.; Dahl, S.; Norskov, J. K.; Chorkendorff, I. *Phys. Chem. Chem. Phys.* **2012**, *14*, 76.
(4) Zhu, S. Q.; Shao, M. H. *J. Solid State Electrochem.* **2016**, *20*, 861.
(5) Feng, X. F.; Jiang, K. L.; Fan, S. S.; Kanan, M. W. *ACS Cent. Sci.* **2016**, *2*, 169.
(6) Ma, S. C.; Sadakiyo, M.; Luo, R.; Heima, M.; Yamauchi, M.; Kenis, P. J. A. *J. Power Sources* **2016**, *301*, 219.
(7) Mistry, H.; Varela, A. S.; Kuhl, S.; Strasser, P.; Cuenya, B. R. *Nat. Rev. Mater.* **2016**, *1*, 16009.
(8) Ji, J. Y.; Zhang, L. L.; Ji, H. X.; Li, Y.; Zhao, X.; Bai, X.; Fan, X. B.; Zhang, F. B.; Ruoff, R. S. *ACS Nano* **2013**, *7*, 6237.
(9) Garg, G.; Basu, S. *Electrochim. Acta* **2015**, *177*, 359.
(10) Hoang, T. T. H.; Gewirth, A. A. *ACS Catal.* **2016**, *6*, 1159.
(11) Andricacos, P. C.; Uzoh, C.; Dukovic, J. O.; Horkans, J.; Deligianni, H. *IBM J. Res. Dev.* **1998**, *42*, 567.
(12) Schlesinger, M.; Paunovic, M. *Modern electroplating*, 5th ed.; Wiley: Hoboken, NJ, 2010.
(13) Lim, R. J.; Xie, M. S.; Sk, M. A.; Lee, J. M.; Fisher, A.; Wang, X.; Lim, K. H. *Catal. Today* **2014**, *233*, 169.
(14) Kapoor, A.; Viraraghavan, T. *J. Environ. Eng.* **1997**, *123*, 371.
(15) Polatides, C.; Kyriacou, G. *J. Appl. Electrochem.* **2005**, *35*, 421.
(16) Gattrell, M.; Gupta, N.; Co, A. *J. Electroanal. Chem.* **2006**, *594*, 1.
(17) Bouzek, K.; Paidar, M.; Sadilkova, A.; Bergmann, H. *J. Appl. Electrochem.* **2001**, *31*, 1185.
(18) Kuhl, K. P.; Cave, E. R.; Abram, D. N.; Jaramillo, T. F. *Energy Environ. Sci.* **2012**, *5*, 7050.
(19) Hori, Y. In *Modern Aspects of Electrochemistry*; Vayenas, C. G., White, R. E., Gamboa-Aldeco, M. E., Eds.; Springer: New York, NY, 2008; p 89.
(20) Kortlever, R.; Shen, J.; Schouten, K. J. P.; Calle-Vallejo, F.; Koper, M. T. M. *J. Phys. Chem. Lett.* **2015**, *6*, 4073.
(21) Wu, J. J.; Zhou, X. D. *Chinese J. Catal* **2016**, *37*, 999.
(22) Jhong, H. R.; Ma, S. C.; Kenis, P. J. A. *Curr. Opin. Chem. Eng.* **2013**, *2*, 191.
(23) Dutta, A.; Rahaman, M.; Luedi, N. C.; Broekmann, P. *ACS Catal.* **2016**, *6*, 3804.
(24) Davies, G. J.; Zhen, S. *J. Mater. Sci.* **1983**, *18*, 1899.
(25) Zhang, W. B.; Ding, C.; Wang, A. J.; Zeng, Y. W. *J. Electrochem. Soc.* **2015**, *162*, D365.
(26) Shin, H. C.; Liu, M. L. *Chem. Mater.* **2004**, *16*, 5460.
(27) Kas, R.; Hummadi, K. K.; Kortlever, R.; de Wit, P.; Milbrat, A.; Luiten-Olieman, M. W. J.; Benes, N. E.; Koper, M. T. M.; Mul, G. *Nat. Commun.* **2016**, *7*, 10748.
(28) Kas, R.; Kortlever, R.; Milbrat, A.; Koper, M. T. M.; Mul, G.; Baltrusaitis, J. *Phys. Chem. Chem. Phys.* **2014**, *16*, 12194.
(29) Li, C. W.; Kanan, M. W. *J. Am. Chem. Soc.* **2012**, *134*, 7231.
(30) Manthiram, K.; Beberwyck, B. J.; Aivisatos, A. P. *J. Am. Chem. Soc.* **2014**, *136*, 13319.
(31) Mistry, H.; Varela, A. S.; Bonifacio, C. S.; Zegkinoglou, I.; Sinev, I.; Choi, Y. W.; Kisslinger, K.; Stach, E. A.; Yang, J. C.; Strasser, P.; Cuenya, B. R. *Nat. Commun.* **2016**, *7*, 12123.
(32) Ma, M.; Djanashvili, K.; Smith, W. A. *Angew. Chem., Int. Ed.* **2016**, *55*, 6680.
(33) Shin, H. C.; Dong, J.; Liu, M. L. *Adv. Mater.* **2003**, *15*, 1610.
(34) Hatch, J. J.; Willey, M. J.; Gewirth, A. A. *J. Electrochem. Soc.* **2011**, *158*, D323.
(35) Efimenko, I. A.; Shishilov, O. N. *Russ. J. Inorg. Chem.* **2012**, *57*, 1695.
(36) Vandenbrande, P.; Winand, R. *Surf. Coat. Technol.* **1992**, *52*, 1.
(37) Witten, T. A.; Sander, L. M. *Phys. Rev. Lett.* **1981**, *47*, 1400.
(38) Godorr, S. A.; Young, B. D.; Bryson, A. W. *Chem. Eng. Commun.* **1992**, *117*, 307.
(39) Russ, J. C. *Fractal surfaces*; Plenum Press: New York, 1994.
(40) Biesinger, M. C.; Lau, L. W. M.; Gerson, A. R.; Smart, R. S. C. *Appl. Surf. Sci.* **2010**, *257*, 887.
(41) Zhu, C. Q.; Osherov, A.; Panzer, M. J. *Electrochim. Acta* **2013**, *111*, 771.
(42) Yin, M.; Wu, C. K.; Lou, Y. B.; Burda, C.; Koberstein, J. T.; Zhu, Y. M.; O'Brien, S. *J. Am. Chem. Soc.* **2005**, *127*, 9506.
(43) Wu, G. Y.; Bae, S. E.; Gewirth, A. A.; Gray, J.; Zhu, X. D.; Moffat, T. P.; Schwarzacher, W. *Surf. Sci.* **2007**, *601*, 1886.
(44) Yu, L.; Akolkar, R. *J. Electrochem. Soc.* **2016**, *163*, D247.
(45) Stewart, K. L.; Gewirth, A. A. *Langmuir* **2007**, *23*, 9911.
(46) Lefebvre, L. P.; Banhart, J.; Dunand, D. C. *Adv. Eng. Mater.* **2008**, *10*, 775.
(47) Giani, L.; Groppi, G.; Tronconi, E. *Ind. Eng. Chem. Res.* **2005**, *44*, 4993.
(48) Liu, Y.; Bliznakov, S.; Dimitrov, N. *J. Phys. Chem. C* **2009**, *113*, 12362.
(49) Kim, D.; Lee, S.; Ocon, J. D.; Jeong, B.; Lee, J. K.; Lee, J. *Phys. Chem. Chem. Phys.* **2015**, *17*, 824.
(50) Ma, S.; Luo, R.; Moniri, S.; Lan, Y. C.; Kenis, P. J. A. *J. Electrochem. Soc.* **2014**, *161*, F1124.
(51) Ma, S. C.; Lan, Y. C.; Perez, G. M. J.; Moniri, S.; Kenis, P. J. A. *ChemSusChem* **2014**, *7*, 866.
(52) Schouten, K. J. P.; Kwon, Y.; van der Ham, C. J. M.; Qin, Z.; Koper, M. T. M. *Chem. Sci.* **2011**, *2*, 1902.
(53) Montoya, J. H.; Shi, C.; Chan, K.; Norskov, J. K. *J. Phys. Chem. Lett.* **2015**, *6*, 2032.

DOI: 10.1021/acscatal.6b03613
ACS Catal. 2017, 7, 3313−3321

(54) Schouten, K. J. P.; Qin, Z. S.; Gallent, E. P.; Koper, M. T. M. *J. Am. Chem. Soc.* **2012**, *134*, 9864.
(55) Hori, Y.; Takahashi, I.; Koga, O.; Hoshi, N. *J. Mol. Catal. A: Chem.* **2003**, *199*, 39.
(56) Ren, D.; Deng, Y. L.; Handoko, A. D.; Chen, C. S.; Malkhandi, S.; Yeo, B. S. *ACS Catal.* **2015**, *5*, 2814.
(57) Durand, W. J.; Peterson, A. A.; Studt, F.; Abild-Pedersen, F.; Norskov, J. K. *Surf. Sci.* **2011**, *605*, 1354.

DOI: 10.1021/acscatal.6b03613
ACS Catal. 2017, 7, 3313−3321